A method for tuning the stiffness of building blocks for statically balanced compliant ortho-planar mechanisms

Blad, T. W.A.; van Ostayen, R. A.J.; Tolou, N.

DOI
10.1016/j.mechmachtheory.2021.104333

Publication date
2021

Document Version
Final published version

Published in
Mechanism and Machine Theory

Mechanism and Machine Theory 162 (2021) 104333

Contents lists available at ScienceDirect

Mechanism and Machine Theory

journal homepage: www.elsevier.com/locate/mechmachtheory

A method for tuning the stiffness of building blocks for statically balanced compliant ortho-planar mechanisms

T.W.A. Blad*, R.A.J. van Ostayen, N. Tolou

Department of Precision and Microsystems Engineering, Delft University of Technology, 2628 CD Delft, the Netherlands

ARTICLE INFO

Article history:
Received 16 September 2020
Revised 21 December 2020
Accepted 11 March 2021

Keywords:
Compliant mechanisms
Ortho-planar mechanisms
Static balancing
Buckling

ABSTRACT

In this paper a method is demonstrated for tuning the stiffness of building blocks for statically balanced compliant ortho-planar mechanisms. Three post-buckled mechanisms are proposed where the flexural rigidity can be manipulated over a part of their length in order to tune the ratio between the first two critical loads. A sensitivity analysis using finite element simulation showed that the best balancing performance is obtained in these mechanisms when this ratio was maximized. The results were validated experimentally by capturing the force-deflection relations.

1. Introduction

Compliant ortho-planar mechanisms (COMs) are planar mechanisms that allow out-of-plane motion through the deflection of flexible members [1]. The advantages of COMs over their conventional counterparts are the ease of their manufacturing process, their compactness and resistance to wear [2]. At the scale of microelectromechanical systems (MEMS) these mechanisms can be applied in accelerometers [3], actuators [4] and micro energy harvesters [5,6]. However, a disadvantage of miniaturized compliant mechanisms is that a significant part of the input energy is stored as strain energy in the deflecting flexible components [7]. This can lead to a low range of motion, poor mechanical efficiency and high natural frequencies [8]. Especially for micro energy harvesting applications, these drawbacks can greatly reduce the overall efficiency [9].

In order to overcome this problem, the stiffness of the mechanism can be reduced by static balancing. Static balancing uses a negative stiffness element as a balancer that counteracts the positive stiffness of the mechanism. As a result, zero stiffness can be obtained over a certain working range if the positive stiffness is of the same magnitude as the negative stiffness [10]. Negative stiffness can be obtained in compliant mechanisms by preloading a flexible element in postbuckling [11]. A MEMS gravimeter is demonstrated by Middlemiss et al. [12] that features a proof mass on top of an anti-spring mechanism. With increasing displacement, the anti-spring softened and the system was able to reach a resonant frequency of 2.3 Hz in the vertical orientation. Another statically balanced compliant mechanism (SBCM) was developed and studied by Tolou et al. [13]. This mechanism was fabricated using deep reactive-ion etching and achieved a near zero stiffness characteristic over a small range of motion. Kuppens et al. [14] demonstrated a SBCM in which the preloading was induced by a MEMS compatible thin film process. The resulting mechanism combined the positive stiffness of a linear guidance mechanism with a postbuckled flexure to achieve static balancing.

* Corresponding author.
E-mail address: t.w.a.blad@tudelft.nl (T.W.A. Blad).

https://doi.org/10.1016/j.mechmachtheory.2021.104333

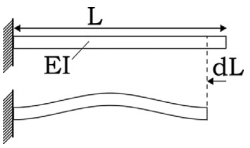

Fig. 1. Slender beam with a uniform cross-section that can be preloaded in the axial direction to achieve the buckled shape extending out of plane.

However, all these SBCMs had a degree of freedom (DOF) in the plane from which they were manufactured, resulting in missing out on the advantages of COMs. In this work, a method is presented to tune the stiffness of mechanisms that can be used as buckling blocks in the design of statically balanced compliant ortho-planar mechanisms (SBCOMs).

In Section 2 the method is introduced for tuning the stiffness of mechanisms consisting of post-buckled beams. Furthermore, the mechanical design of the prototypes and the experimental methods are discussed. The results are shown in Section 3 and discussed in Section 4. Section 5 lists the most important conclusions.

2. Methods

2.1. Buckling of a slender beam

Fig. 1 schematically depicts a slender beam with a uniform cross section with a length, L, and flexural rigidity of EI. The initially flat beam can be buckled by compressing the beam over a distance of dL, a process which is called preloading and results in the beam assuming a post-buckled shape that extends out of plane. The out-of-plane displacement as a function of the axial coordinate, $y(x)$, corresponding to an applied axial load, P, is governed by the following differential equation [15].

$$\frac{d^4y}{dx^4} + \frac{P}{EI}\frac{d^2y}{dx^2} = 0 \tag{1}$$

Where EI is the flexural rigidity of the section which is a combination of the elastic modulus, E, and the second moment of inertia around the bending axis, I. This is a homogeneous fourth-order differential equation for which the general solution is given as follows.

$$y(x) = A\sin\left(\frac{\lambda}{\sqrt{EI}}x\right) + B\cos\left(\frac{\lambda}{\sqrt{EI}}x\right) + Cx + D \tag{2}$$

Where A,B,C,D are unknown constants that depend on the boundary conditions of the beam and λ are the eigenvalues corresponding to the critical loads of the beam such that $\lambda^2 = P_{\text{crit}}$. These critical loads are the compressive loads at which the system will lose stability and buckle. Any continuous system has an infinite number of critical loads, $P_{\text{crit},i}$, where i denotes the number of the critical load and corresponding buckling mode. The critical loads are ordered by increasing magnitude such that the first critical load, $P_{\text{crit},1}$, is the load corresponding to lowest value. The transcendental eigenvalue problem can be expressed by the following equation [16].

$$\mathbf{T}(\lambda)\mathbf{z} = 0 \tag{3}$$

Where $\mathbf{T}$ is a matrix consisting of transcendental functions in λ, and $\mathbf{z}$ is a constant eigenvector containing A,B,C,D. The critical loads of the beam are represented by the non-trivial solutions of λ for $\mathbf{z} \neq 0$, and the mode shapes can be found by substituting the result in (2). Solving this eigenvalue problem for a beam with fixed boundary conditions at both ends yields the following first and second critical loads.

$$P_{crit,1} = \frac{(2\pi)^2 EI}{L^2}, \quad P_{crit,2} = \frac{(2.85\pi)^2 EI}{L^2}, \tag{4}$$

When the preload is applied, the axial force, P, on the beam rapidly increases until the first critical load is reached and the beam begins to buckle. Due to the slenderness of the beam the critical load is reached almost instantly [17]. Beyond the point of buckling, the axial force remains equal to the first critical load and the displacement field of the beam is described by the first buckling mode, which is the lowest energy configuration. In this configuration the beam is in a stable equilibrium where the potential energy, $E_{eq,stable}$, is equal to the work done by the preloading, W, which can be found by the following equation.

$$\mathrm{W} = \int_0^{dL} P\mathrm{dx} \approx P_{\text{crit},1}dL \tag{5}$$

When the beam is actuated in the out-of-plane direction, an unstable equilibrium can be found where the displacement field of the beam is described by the second buckling mode. Similar to the stable equilibrium, the axial force (i.e. the reaction force on the fixed boundary condition) is equal to the second critical load in this configuration [18]. Moreover,

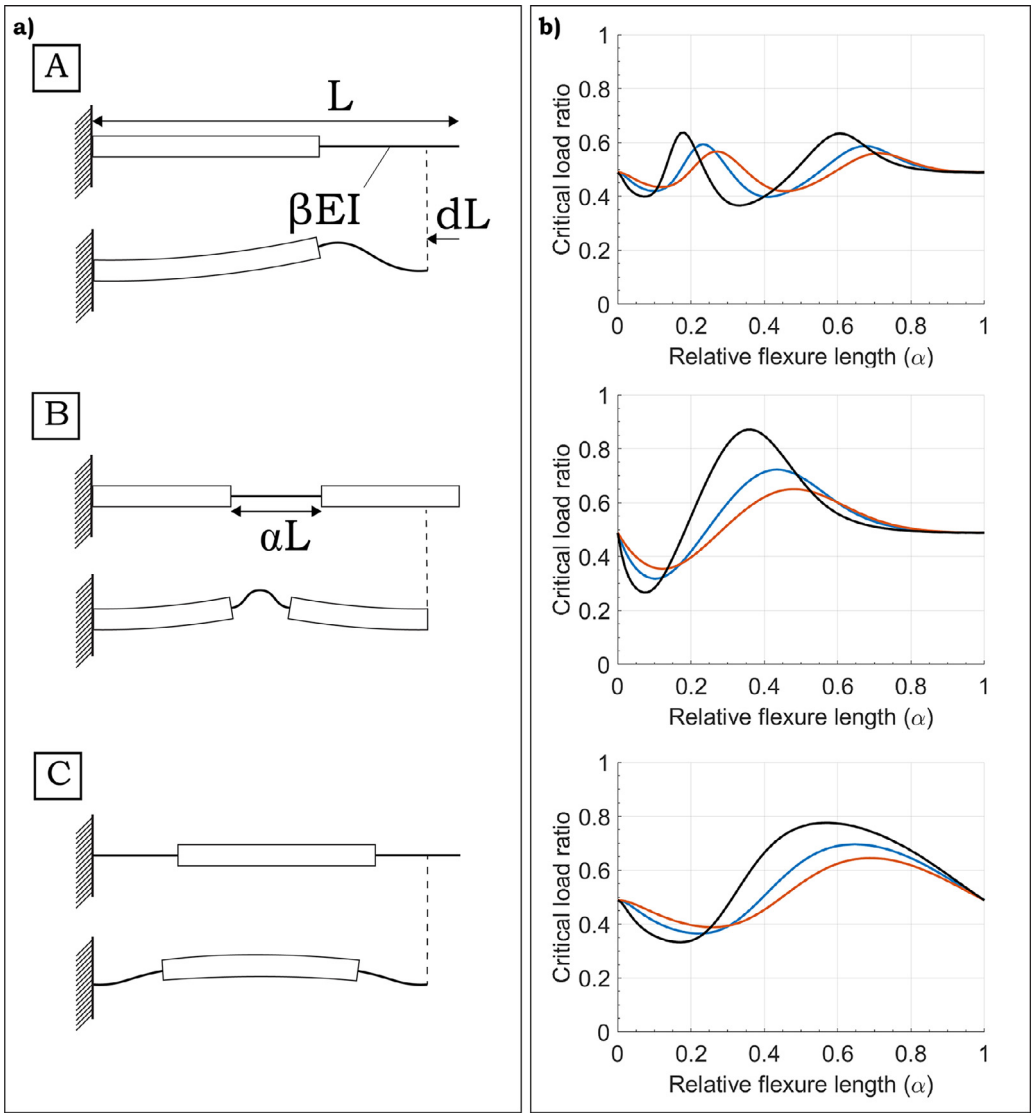

Fig. 2. a) Proposed mechanisms (A, B, C) in unloaded and post-buckled configurations and b) their critical load ratios as a function of the design parameters $\boldsymbol{\alpha}$ and $\boldsymbol{\beta}$;
$\boldsymbol{\beta} = 0.1$, $\boldsymbol{\beta} = 0.2$, $\boldsymbol{\beta} = 0.3$.

the potential energy in this configuration is equal to the work that would be required to preload the beam in the second buckling mode, $E_{eq,unstable} \approx P_{\text{crit},2} dL$.

Therefore, the ratio between the critical loads corresponding to the buckling modes that describe the displacement fields in the stable and unstable equilibria is an important measure to identify the variation of potential energy in the buckled system. This variable is proposed as the *critical load ratio, CLR,* and can for these beams be found as the ratio between the first and second critical load.

$$CLR = \frac{P_{\text{crit},1}}{P_{\text{crit},2}} \tag{6}$$

For the uniform beam it can be found that the $CLR = 0.49$ and is independent of the geometry of the beam. However, by locally manipulating the flexural rigidity of the beam, the *CLR* can be tuned. As the *CLR* approaches unity, the potential energy in the stable and unstable equilibria converge to the same value and therefore static balancing is achieved.

2.2. Mechanisms for tuning the critical load ratio

In order to tune the *CLR*, the three mechanisms shown in Fig. 2a are proposed. The mechanisms have the same length, L, but their cross-sections are modified such that over a fraction of their length, αL, where $0 < \alpha < 1$, the flexural rigidity is

Table 1
Relevant parameters of the manufactured prototypes.

Fixed parameter	Symbol	Value
Unloaded device length	L	20 mm
Axial load displacement	dL	0.4 mm
Width of wide segments	w	2 mm
Width of narrow segments	w_f	0.2 mm
Thickness of mechanism	t	100 μm
Design variables	$\boldsymbol{\alpha}$	$\boldsymbol{L_f}$
Flexure length A1	0.177	3.54 mm
Flexure length A2	0.605	12.10 mm
Flexure length B	0.361	7.22 mm
Flexure length C	0.563	5.63 mm (each)

reduced to βEI, where $0 < \beta < 1$. The portions over which the flexural rigidity of the mechanisms is reduced will be called the flexures. In Mechanism A, a single flexure is positioned at the end of the beam; in Mechanism B, a single flexure is positioned in the middle of the beam; and in Mechanism C, two flexures are positioned at the ends of the beam, with each a length $\frac{\alpha L}{2}$.

Mechanisms A, B, and C can be considered as stepped beams with segments of varying lengths and cross-sections in series. The length can be divided in N segments with $x_{n-1} < x < x_n$ for $n = 1 : N$ such that $x_0 = 0$ and $x_N = L$. Moreover, the flexural rigidity of section n is defined as EI_n. The solution to (1) now becomes a set of N homogeneous fourth-order differential equations with the form of (2) including the unknown constants A_n, B_n, C_n, D_n. The fixed boundary conditions at the ends remain, and at the intermediate boundaries between the segments the boundary conditions are found by enforcing continuity and balancing the forces and bending moments. These boundary conditions are formulated as follows.

$$\begin{aligned} &y_n(x_n) = y_{n+1}(x_n),\ \frac{dy_n}{dx}(x_n) = \frac{dy_{n+1}}{dx}(x_n), \\ &\frac{d^2y_n}{dx^2}(x_n) = \frac{d^2y_{n+1}}{dx^2}(x_n),\ \frac{d^3y_n}{dx^3}(x_n) = \frac{d^3y_{n+1}}{dx^3}(x_n) \end{aligned} \tag{7}$$

The critical loads can again be found as the non-trivial solutions of λ for $\mathbf{z} \neq 0$ of the transcendental eigenvalue problem of (3). In this case, the *CLR* is a function of only the relative lengths and flexural rigidities of the beam segments, which are defined by the parameters α and β. In Fig. 2b, the *CLR* is plotted for Mechanisms A, B and C as a function of α for three variations of β.

2.4. Mechanical design

The mechanisms from Fig. 2a are prototyped from 0.1 mm thick spring steel ($E = 190$ GPa) using a Spectra-Physics Talon 355–15 diode pumped solid-state (DPSS) UV laser system with a wavelength of 355 nm and maximum power of 15 W at 50 kHz and are shown in Fig. 4A. The relative difference in flexural rigidity was fixed at $\beta = 0.1$, which was realized by manipulating the width of the beam. For all mechanisms the following parameters were fixed: the unloaded length, L, the applied axial displacement, dL, the width of the wide segments, w, the width of the narrow segments (i.e. flexures), w_f, and the thickness, t. The mechanisms were fabricated with flexure lengths, L_f, such that the relative lengths of the flexures, α, correspond to the maxima in *CLR* found in Fig. 2b. For Mechanism A, two maxima were found in the *CLR* and therefore two prototypes were manufactured. These prototypes will be named A1, corresponding to the optimum with a short flexure and A2, corresponding to the optimum with a long flexure. For each mechanism, a sensitivity analysis is carried out using finite element simulation around the maxima in the *CLR*, and their force-deflection characteristics were measured experimentally. All parameters are depicted in Fig. 3 and summarized in Table 1.

The beams were clamped in an aluminum frame consisting of a base plate and two sliding sides. The sides are aligned using dowel pins and can be clamped to the base by tightening the bolts on the sides. The assembly process was as follows. First, a spacer with a thickness of 0.4 mm was placed between the sides and the base of the frame and the bolts were tightened. Next, the beam was mounted to the frame by clamping it between the aluminum and a PMMA bracket. In this state the beam is stress-free and therefore not buckled. Next, the bolt on the side is released such that the spacer can be removed and is subsequently tightened again such that the sides of the frame have moved exactly the thickness of the spacer compared to the stress-free configuration. This introduces an axial preload and the beam should buckle out of plane to one of its stable positions. The assembled structure is shown in Fig. 4C.

2.5. Finite element model

To simulate the mechanical behavior of the post-buckled beams a finite element model was built in ANSYS using beam elements (beam188). The material is assumed to be perfectly elastic with the following properties ($E = 190$ GPa, $\nu = 0.34$, $\rho = 7.82\,\mathrm{g/cm^3}$). Buckling was induced by constraining one end of the beam in all directions, and displacing the other

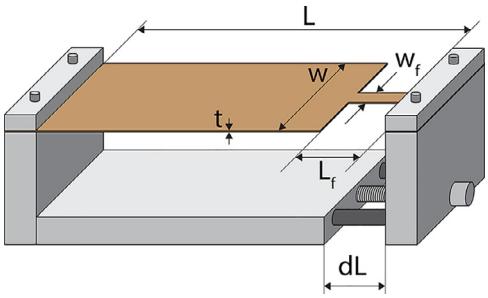

Fig. 3. Schematic showing the important dimensions of the prototype of Mechanism A in the unloaded position. From this configuration an axial load is applied to induce the buckling of the beam.

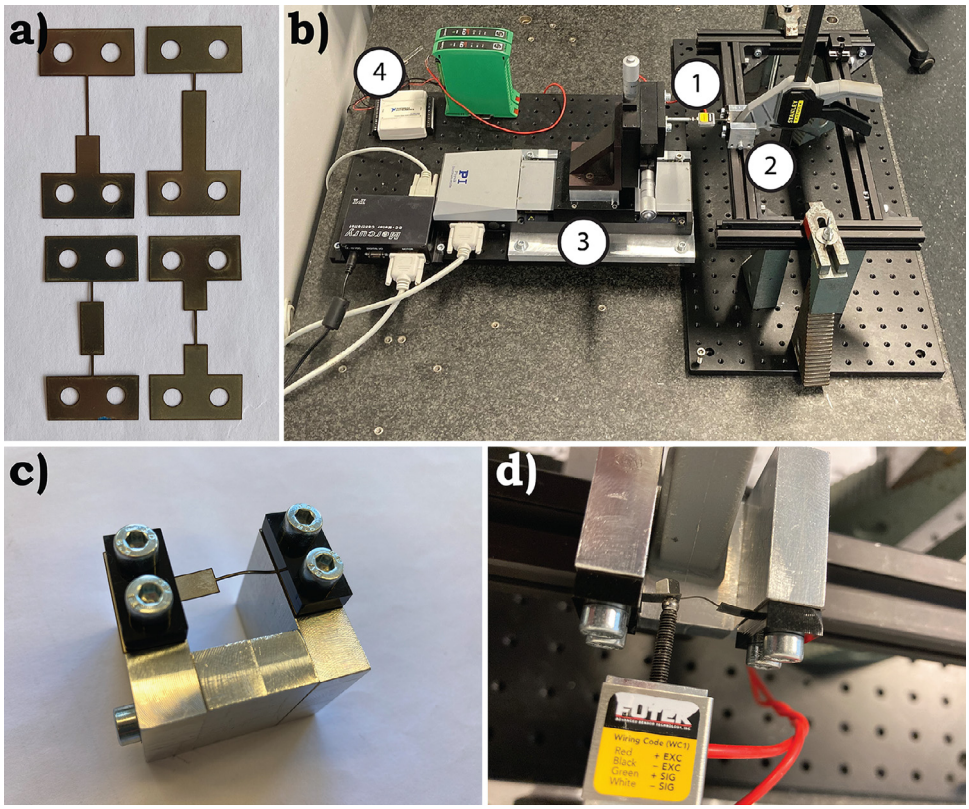

Fig. 4. Mechanical design of a) the fabricated mechanisms and c) assembled prototype using a frame to apply axial loading and induce buckling and experimental setup for evaluation of force-deflection behavior; b) overview of components d) close-up of rolling contact and magnet at the interface of the flexure to ensure contact in the unstable region.

end. Small imperfections were incorporated in the model to prevent the simulation to crash due to singularities in this preloading step. After the buckled shape was achieved, a displacement was applied at the interface of the flexure. During this the reaction forces are recorded at regular intervals to determine the force-deflection behavior.

2.6. Experimental characterization

The force-deflection characteristics of the beams were evaluated experimentally with the setup shown in Fig. 4B. For this a FUTEK LRM200 force sensor (1) is connect to the prototype (2) and displaced by a PI M-505 motion stage (3) from which the internal encoder captures position data. Data was recorded using a NI USB-6008 (4) in 100 steps with a resolution of 100 μm. The probe is fixed to the beam at the interface of the flexure using a rolling contact and a magnet as shown in Fig. 4D. This ensures that the probe will remain in contact with the system in the unstable region.

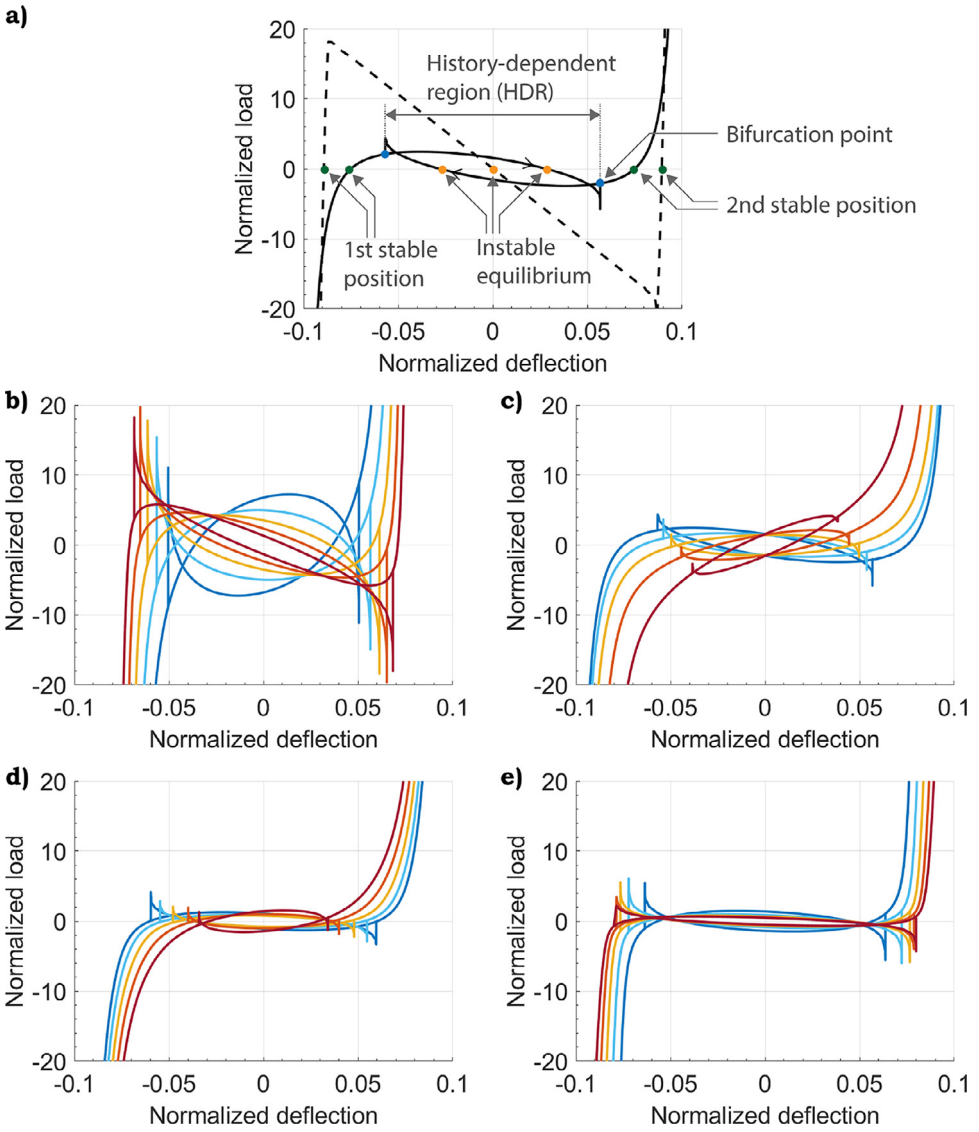

Fig. 5. a) Identification of important points in the normalized load-deflection relation for uniform beam (▬ ▬) and Mechanism A2 (▬). b–e) Sensitivity analysis of normalized load-deflection relations of b) Mechanism A1, c) Mechanism A2, d) Mechanism B, and e) Mechanism C. The relative flexure length α is varied around the optima found in Fig. 2b;
▬ $\alpha = 0.8\,\alpha_{opt}$, ▬ $\alpha = 0.9\,\alpha_{opt}$, ▬ $\alpha = \alpha_{opt}$, ▬ $\alpha = 1.1\,\alpha_{opt}$, ▬ $\alpha = 1.2\,\alpha_{opt}$. .

3. Results

In Fig. 5, the force-deflection relations resulting from the simulations are shown for the normalized load ($\tilde{F} = \frac{FL^2}{EI}$) and normalized deflection ($\tilde{d} = \frac{d}{L}$). Fig. 5a shows the relations of the uniform beam and Mechanism A2 and identifies important characteristics of the curve. Fig. 5b–e show the relations for variations in parameter α in Mechanisms A1, A2, B and C, respectively. The relative flexure length is varied by +/- 10% and +/- 20% around the optimum in *CLR* for each mechanism as shown in Fig. 2. In Fig. 6, the measured force-deflection relations are shown. In Table 1. Relevant parameters of the manufactured prototypes

Table 2 the first two critical loads and the *CLR* is shown for the Mechanisms A1, A2, B and C at the optimum in *CLR* for each mechanism as shown in Fig. 2.

4. Discussion

4.1. Force-deflection relation of buckled mechanisms

The nonlinear force-deflection relations of the post-buckled mechanisms shown in Figs. 5 and 6 are characterized by the points identified in Fig. 5a. These include two stable equilibrium positions and one or more unstable equilibria. It can

Table 2
First two critical loads and ***CLR*** of the mechanisms for the optima found in Fig. 2b.

Mechanism	$P_{crit,1}$ [N]	$P_{crit,2}$ [N]	*CLR*
A1	4.78	7.51	0.64
A2	1.64	2.6	0.64
B	3.24	3.72	0.88
C	2.07	2.67	0.78

be observed that between the stable equilibria the mechanisms are relatively compliant, and the force-deflection relation rapidly steepens for larger displacements. This steepening effect is a result of the mechanisms being straightened and loaded in tension. In the force-deflection relations of the mechanisms, two bifurcation points can be identified between which two load paths are present, corresponding to the two configurations of the mechanisms that can be identified as "knee-up" and "knee-down". This section of the curve between the bifurcation points is identified as the history-dependent region (HDR). When actuated from one side to the other, there is a point where the mechanisms experience a snap-through bi-stability and change configuration. The two load paths in the HDR are a result of the series configurations of the mechanism topologies and are not observed in the parallel topology used by Kuppens et al. [14]. The main difference is the rotational degree of freedom at the point where the force-deflection relation is measured.

Depending on the mechanism, there is a potential barrier which has to be overcome before the snap-through occurs. This is especially evident in Mechanism A1, and can be seen from the sharp peaks in the force-deflection relation close to the bifurcation points. In the other mechanisms, these peaks are smaller, which indicates that for these mechanisms the potential barrier is lower. Moreover, the area between the load paths in the HDR also varies for each mechanism. It can be seen that for Mechanism C the load paths are relatively close together, and for Mechanism A1 the load paths enclose a much larger area. The size of this area is a measure for the energy captured in the system before the snap-through [18]. When the load paths are further apart, more energy is required to actuate the mechanism and less balancing performance is obtained.

4.2. Critical load ratio and force-deflection relation

Drawing a line between the bifurcation points finds a general trend in the slope of the HDR, which can slope upwards, slope downwards or can be relatively flat. For Mechanisms A2, B and C it can be observed from Fig. 5 that mechanisms with an increasingly upwards sloping HDR are obtained when $\alpha > \alpha_{opt}$ and mechanisms with increasingly downwards sloping HDR are obtained for $\alpha < \alpha_{opt}$. Moreover, for these mechanisms the flattest slope of the HDR is obtained at $\alpha = \alpha_{opt}$ (i.e. where the *CLR* is maximized). Therefore, the *CLR* can in these cases be used as a tool for finding the design variables that lead to a the greatest degree of static balancing. However, in Mechanism A1 the flattest slope was not found at $\alpha = \alpha_{opt}$ and the opposite effect is observed for the slope of the HDR.

Moreover, the value of the *CLR* can also give information on how well the mechanisms can be balanced, as the *CLR* is a measure to identify the variation of potential energy in the buckled system between the stable and the unstable equilibria. Therefore, if a $CLR = 1$ can be achieved a mechanism is expected to be statically balanced between the stable and unstable equilibrium positions. Not all mechanisms can be statically balanced, but in that case it is expected that when the *CLR* is maximized a design is obtained with a load-deflection relation closest to statically balanced. It can be observed that the maxima of the *CLR* curves have greater values for Mechanisms B and C compared to A1 and A2. As a result, these mechanisms have their load paths closer together, require lower actuation forces and therefore show a better balancing performance.

However, it is important to note that the *CLR* only gives a ratio between the variation of potential energy, and it is important to consider the actual values of the critical loads too. As can be found from.

Table 2, the critical loads of Mechanisms A1 and B are greater than the critical loads of Mechanisms A2 and C, respectively. Therefore, the *CLR* of A1 and A2 may be quite similar while A2 clearly shows a better balancing performance. A similar results was found for Mechanisms B and C, where the *CLR* of B is higher, but due to the lower critical loads a better balancing performance is found in C.

4.3. Usage of the beams as building blocks for SBCOMs

When the Mechanisms A, B, C are to be used as building blocks for SBCOMs, it is necessary to prevent the rotation of the actuation point to achieve $CLR = 1$ and the desired static balancing. This can for example be achieved by designing an ortho-planar platform by arranging three of these mechanisms in a rotationally symmetric way and connecting their actuation points. As a result, the rotation is prevented by the added stiffnesses of the two other elements. However, this arrangement requires some modifications to the building blocks in order to relax the in-plane displacements at the actuation point to prevent over-constraints.

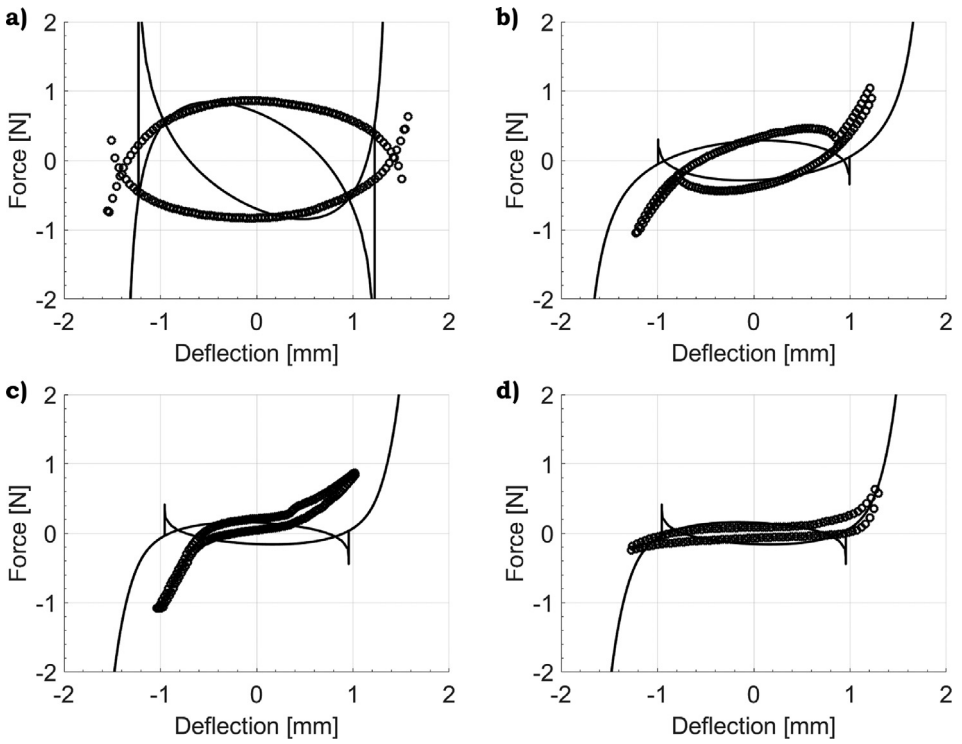

Fig. 6. Simulated (▬) and measured (O) force-deflection relations of a) Mechanism A1, b) Mechanism A2, c) Mechanism B and d) Mechanism C.

5. Conclusions

In this paper we have proposed and demonstrated a method to tune the force-deflection behavior of buckled mechanisms based on a linear buckling analysis. Through locally manipulating the flexural rigidity of a beam over part of its length, the ratio between the first two critical loads of the mechanism can be tuned. Maximizing this ratio results in the best balancing performance for a given mechanism. A sensitivity analysis was conducted through finite element simulation and the results were validated experimentally. These proposed mechanisms can be used building blocks for statically balanced compliant ortho-planar mechanisms.

Declaration of Competing Interest

The authors declare that they have no known competing financial interests or personal relationships that could have appeared to influence the work reported in this paper.

Funding

This work is part of the research programme Rethinking Energy Harvesting for MEMS (REH-MEMS) with project number 14379, which is financed by the Stichting voor de Technische Wetenschappen (STW) and the Netherlands organisation for Scientific Research (NWO).

References

[1] J.J. Parise, L.L. Howell, S.P. Magleby, Ortho-planar linear-motion springs, Mech. Mach. Theory 36 (2001) 1281–1299, doi:10.1016/S0094-114X(01)00051-9.
[2] L.L. Howell, Compliant mechanisms, in: J.M. McCarthy (Ed.), Proceedings of the 21st Century Kinematics, Springer, 2013, pp. 189–216.
[3] H. Dong, Y. Jia, Y. Hao, S. Shen, A novel out-of-plane MEMS tunneling accelerometer, Sens. Actuators Phys. 120 (2005) 360–364, doi:10.1016/j.sna.2004.12.021.
[4] S. He, R.B. Mrad, Design, modeling, and demonstration of a MEMS repulsive-force out-of-plane electrostatic micro actuator, J. Microelectromechanical Syst. 17 (2008) 532–547, doi:10.1109/JMEMS.2008.921710.
[5] K. Tao, S.W. Lye, J. Miao, L. Tang, X. Hu, Out-of-plane electret-based MEMS energy harvester with the combined nonlinear effect from electrostatic force and a mechanical elastic stopper, J. Micromechanics Microengineering 25 (2015) 104014, doi:10.1088/0960-1317/25/10/104014.
[6] M. Han, Q. Yuan, X. Sun, H. Zhang, Design and fabrication of integrated magnetic MEMS energy harvester for low frequency applications, J. Microelectromechanical Syst. 23 (2014) 204–212, doi:10.1109/JMEMS.2013.2267773.
[7] J.A. Gallego, J.L. Herder, in: Criteria For the Static Balancing of Compliant Mechanisms., American Society of Mechanical Engineers Digital Collection, 2011, pp. 465–473.

[8] N. Tolou, V.A. Henneken, J.L. Herder, in: Statically Balanced Compliant Micro Mechanisms (SB-MEMS): Concepts and Simulation., American Society of Mechanical Engineers Digital Collection, 2011, pp. 447–454.
[9] T.W. Blad, N. Tolou, On the efficiency of energy harvesters: a classification of dynamics in miniaturized generators under low-frequency excitation, J. Intell. Mater. Syst. Struct. 30 (2019) 2436–2446, doi:10.1177/1045389X19862621.
[10] K. Hoetmer, J.L. Herder, C.J. Kim, in: A Building Block Approach for the Design of Statically Balanced Compliant Mechanisms., American Society of Mechanical Engineers Digital Collection, 2010, pp. 313–323.
[11] M. Schenk, S.D. Guest, On zero stiffness, Proc. Inst. Mech. Eng. Part C J. Mech. Eng. Sci. 228 (2014) 1701–1714, doi:10.1177/0954406213511903.
[12] R.P. Middlemiss, A. Samarelli, D.J. Paul, J. Hough, S. Rowan, G.D. Hammond, Measurement of the Earth tides with a MEMS gravimeter, Nature 531 (2016) 614–617, doi:10.1038/nature17397.
[13] N. Tolou, P. Estevez, J.L. Herder, in: Collinear-Type Statically Balanced Compliant Micro Mechanism (SB-CMM): Experimental Comparison Between Pre-Curved and Straight Beams., American Society of Mechanical Engineers Digital Collection, 2012, pp. 113–117.
[14] P.R. Kuppens, J.L. Herder, N. Tolou, Permanent stiffness reduction by thermal oxidation of silicon, J. Microelectromechanical Syst. 28 (2019) 900–909, doi:10.1109/JMEMS.2019.2935379.
[15] S.P. Timoshenko, J.M. Gere, Theory of Elastic Stability, Courier Corporation, 2009 ISBN 978-0-486-47207-2.
[16] K.V. Singh, G. Li, Buckling of functionally graded and elastically restrained non-uniform columns, Compos. Part B Eng. 40 (2009) 393–403, doi:10.1016/j.compositesb.2009.03.001.
[17] B. Camescasse, A. Fernandes, J. Pouget, Bistable buckled beam and force actuation: experimental validations, Int. J. Solids Struct. 51 (2014) 1750–1757, doi:10.1016/j.ijsolstr.2014.01.017.
[18] P. Cazottes, A. Fernandes, J. Pouget, M. Hafez, Bistable buckled beam: modeling of actuating force and experimental validations, J. Mech. Des. (2009) 131, doi:10.1115/1.3179003.